

Horizon 2020 Program (2014-2020)
FET-Open Novel ideas for radically new technologies
FETOPEN-01-2018-2019-2020



Architecting More than Moore – Wireless Plasticity for
Massive Heterogeneous Computer Architectures †

**D1.3: Tunable and Switchable Graphene Multiantenna
Report**

Contractual Date of Delivery	30/09/2023
Actual Date of Delivery	30/09/2023
Deliverable Security Class	Public
Editor	Elana Santana (UoS)
Contributors	Elana Santana (UoS) Peter Haring Bolívar (UoS)
Quality Assurance	Max Lemme (AMO) Eduard Alarcón (UPC)

† This project is supported by the European Commission under the Horizon 2020 Program with Grant agreement no: 863337

Document Revisions & Quality Assurance

Deliverable Number	D1.3
Deliverable Responsible	UoS
Work Package	WP1
Main Editor	Elana Santana (UoS)

Internal Reviewers

1. Max Lemme (AMO)
2. Eduard Alarcón (UPC)

Revisions

Version	Date	By	Overview
1.3.3	30/09/2023	Elana Santana (UoS)	Report ready for submission
1.3.2	29/09/2023	Elana Santana (UoS)	Minor edits after internal revision
1.3.1	10/09/2023	Elana Santana (UoS)	Update from UoS submitted to internal review
1.3.0	05/09/2023	Elana Santana (UoS)	First draft with UoS contribution.

Legal Disclaimer

The information in this document is provided “as is”, and no guarantee or warranty is given that the information is fit for any particular purpose. The above referenced consortium members shall have no liability to third parties for damages of any kind including without limitation direct, special, indirect, or consequential damages that may result from the use of these materials subject to any liability which is mandatory due to applicable law. © 2019 by WiPLASH Consortium.

Executive Summary

The WiPLASH project aims to develop massive heterogeneous architectures with improved data delivery using graphene-based RF devices for miniaturized, tunable, and ultra-high-speed wireless communications, which can be achieved with the use of graphene antennas working at THz frequencies. One of the main targeted breakthroughs of the project is the experimental validation of graphene-based tunable antennas in the terahertz band. However, an experimental validation of the tunability of graphene-based antennas at THz frequencies remains a challenge due to their very low emission. This is due to the graphene material's intrinsic characteristics – chemical potential and relaxation time - resulting from its manufacturing process, handling, and patterning.

This deliverable is the third and last report from WP1 RF Design and Implementation, and it aims to present simulations of the achievable performance of tunability and beam-steering capabilities of graphene-based multiantenna solutions. Additionally, experimental validation of graphene-based antennas emitting THz radiation and being tunable is also presented. The main contributions of this deliverable are (i) the experimental demonstration of THz emission of an optically excited graphene-based dipole antenna; (ii) the experimental demonstration of THz emission and tunability of an optically excited graphene patch antenna; (iii) the experimental demonstration of THz emission of an all-electronic graphene patch antenna and demonstration of THz tuning possibility; and (iv) simulations of the achievable performance of graphene-based all-electronic patch antenna arrays.

Abbreviations and Acronyms

AUT	Antenna Under Test
CMOS	complementary metal-oxide semiconductor
CVD	Chemical Vapor Deposition
GSG	Ground-signal-ground
hBN	Hexagonal Boron Nitride
HR-Si	High-resistive Silicon
InGaAs	Indium Gallium Arsenide
LT-GaAs	Low-temperature Gallium Arsenide
PCA	Photoconductive Antenna
Rx	Receiver
SiGe	Silicon-Germanium
THz-TDS	Terahertz Time Domain Spectroscopy
Tx	Transmitter
VNA	Vector Network Analyzer

The *WiPLASH* consortium is composed by:

UPC	Coordinator	Spain
IBM	Beneficiary	Switzerland
UNIBO	Beneficiary	Italy
EPFL	Beneficiary	Switzerland
AMO	Beneficiary	Germany
UoS	Beneficiary	Germany
RWTH	Beneficiary	Germany



IBM **Research** | Zurich



Table of Contents

DOCUMENT REVISIONS & QUALITY ASSURANCE	2
EXECUTIVE SUMMARY	3
ABBREVIATIONS AND ACRONYMS	4
TABLE OF CONTENTS	7
LIST OF FIGURES	8
1 INTRODUCTION	10
2 GRAPHENE-BASED ANTENNA MEASUREMENTS.....	12
2.1 OPTICALLY EXCITED GRAPHENE-BASED DIPOLE ANTENNA.....	12
2.2 OPTICALLY EXCITED GRAPHENE-BASED PATCH ANTENNA	15
2.3 ALL-ELECTRONIC EXCITED GRAPHENE-BASED PATCH ANTENNA.....	17
2.3.1 <i>Graphene Monolayer Patch Antenna</i>	18
2.3.2 <i>Graphene Monolayer hBN Embedded Patch Antenna</i>	20
2.3.3 <i>Graphene Stack Patch Antenna</i>	20
3 GRAPHENE-BASED ANTENNA ARRAYS SIMULATIONS	23
4 SUMMARY OF RESULTS	25
BIBLIOGRAPHY	27

List of Figures

Figure 1: THz-TDS measurement setup inside a box for N2 environment measurements	12
Figure 2: Different dipole PCA designs with (a) metal dipole, (b) standard graphene dipole, (c) graphene dipole with graphene conduction lines, and (d) graphene dipole with metal close to dipole gap	13
Figure 3: THz emission measurements of the graphene dipole of Figure 2d with laser excitation spot being in the dipole gap, below and above it with (a) time-domain spectra and (b) frequency-domain spectra	13
Figure 4: Time-domain peak-to-peak value of the THz emission over repetitive measurements	14
Figure 5: Comparison of the THz emission of the graphene dipole before and after 20 measurements with (a) time-domain spectra and (b) frequency-domain spectra.....	14
Figure 6: s-SNOM image of the graphene dipole (a) before and (b) after THz-TDS measurements. Top: Topography, center: E-field amplitude, and bottom: E-field phase	15
Figure 7: InGaAs emitter on top of the graphene patch antenna. The metal line in contact with the graphene patch is used for biasing graphene by gate-tuning	15
Figure 8: THz emission comparison of only InGaAs and InGaAs on top of graphene with (a) time-domain spectra and (b) frequency-domain spectra	16
Figure 9: THz emission comparison of InGaAs on top of graphene with different applied bias with (a) time-domain spectra and (b) frequency-domain spectra	16
Figure 10: InGaAs emitter on top of the exfoliated graphene	17
Figure 11: THz emission comparison of InGaAs on top of exfoliated graphene with different applied bias with (a) time-domain spectra and (b) frequency-domain spectra	17
Figure 12: VNA setup for characterization of all-electronic patch antennas	18
Figure 13: Patch antennas in polyimide substrate with (a) standard metal patch antenna and (b) graphene patch antenna	18
Figure 14: Measured values of (a) S11 and (b) gain of the metal patch antenna.....	19
Figure 15: Measured values of (a) S11 and (b) gain of the graphene patch antenna	19
Figure 16: CVD hBN/CVD graphene/CVD hBN patch antenna.....	20
Figure 17: Measured values of (a) S11 and (b) gain of the graphene embedded in hBN patch antenna	20
Figure 18: Graphene stack patch where (a) is the proposed design and (b) is a demonstration of the graphene tuning.	21
Figure 19: S11 parameter of the patch antenna with graphene of different chemical potentials (that can be modified with the bias) and 1.2ps of relaxation time for (a) a standard monolayer antenna and (b) for the proposed antenna stack.....	21
Figure 20: Efficiency and gain comparison of a standard single layer graphene antenna and the proposed graphene stack	22
Figure 21: Example of the antenna array simulation in CST with (a) single antenna and (b) 2x2 antenna array	23
Figure 22: simulated 3D pattern of the far-field gain of the antenna arrays	23
Figure 23: Simulated 3D far-field pattern for the antenna array when (a) an input phase delay of 20° between antennas and (b) for an input phase delay of 45° between antennas	24

Figure 24: Simulated 3D far-field pattern for the antenna array with 0.3ps of relaxation time when (a) an input phase delay of 20° between antennas and (b) for a input phase delay of 45° between antennas..... 24

1 Introduction

Graphene has been considered one of the main drivers for future 6G wireless communication systems due to its plasmonic characteristics at the THz frequency region [1] [2]. A graphene plasmonic antenna designed for THz frequencies is smaller in dimension compared to its metallic counterpart, which is a big advantage for saving area on a chip scale [3] [4]. Additionally, the unique energy band dispersion relation of graphene allows the tunability of its conductivity and, consequently, its resonance frequency when used as an antenna [5] [6]. Thus, the THz graphene plasmonic antenna can enable THz communications in a variety of frequency bands, which can be chosen by modifying the graphene conductivity electrically or chemically.

The deliverable D1.3 Tunable and Switchable Multiantenna Report is focused on the experimental demonstration of THz emission of graphene antennas, as well as its emission tunability. Even though theoretical and simulation results promise an efficient THz emission and tunability of graphene antennas [7], the experimental validation is until the present day a big challenge. The emission characteristics of a graphene antenna are highly affected by the graphene material [3] [7], which cannot meet the standards of the majority of the simulation studies. While the most published papers regarding graphene antennas at THz frequencies use graphene of around 1 ps of relaxation time [8] [9], this is not usually the case for the standard values obtained by a commercial CVD graphene used for experiments, as can be calculated from Deliverable 2.1 First Co-integration of Graphene Antennas with Full Custom SiGe Transceivers, where the average charge carrier mobility for the graphene used in our experiments is around of 3,000 cm²/Vs. The low quality of CVD graphene limits the performance of graphene antennas and makes the measurements extremely difficult due to the very low emission of these antennas.

For the purpose of being able to measure the very low emission of THz plasmonic graphene antennas and demonstrate its tunability, two different paths were chosen: (i) photoconductive antennas (PCAs) and, (ii) all-electronic antennas. While the PCAs can be characterized by the THz time-domain spectroscopy (THz-TDS) system of UoS up to 2 THz, an all-electronic antenna can be characterized by a vector network analyzer (VNA) with frequency extenders in a smaller bandwidth, in our case from 220 GHz to 325 GHz. The all-electronic antenna is developed to demonstrate a plasmonic graphene antenna that can be easily integrated with Tx/Rx modules. Both PCAs and all-electronic antennas were developed using materials compatible with CMOS technologies.

Two different PCAs were developed, these being (a) a standard graphene dipole PCA, and (b) a graphene patch antenna with an InGaAs emitter. The antenna (a) is the modification of a standard dipole PCA used as a THz emitter in traditional THz-TDS systems. A standard dipole PCA is usually made of metal dipoles deposited on top of a semiconductor, mainly LT-GaAs. The antenna-under-test (AUT) developed and characterized by UoS consists of graphene dipoles deposited on top of a high-resistive silicon (HR-Si) substrate. For this configuration, a voltage bias applied to the dipole is needed for the generation of the THz radiation. The principle is the same as in a standard THz-TDS, where an optical pulse focused in the center of the dipole gap creates electron-hole pairs, which are accelerated to the dipole antenna arms by the applied bias. The movement and recombination of these charges occur in a ps time scale, which translates to a THz emitted signal at the far-field [10].

For the antenna (b), no bias is needed for the THz generation and, in this case, it is possible to use a bias to tune the THz emission. The configuration of the antenna (b) consists of an InGaAs emitter on top of a graphene patch antenna deposited on an HR-Si/SiO₂ substrate. The THz generation in this case is based on the photo-Dember effect, where the movements of the electrons and holes created by an optical excitation are due to the attraction and repulsive forces among the charges and not by a bias voltage [11]. The idea is that the THz radiation emitted by the InGaAs charge carriers couples to the graphene patch below it, which will act as an antenna. The graphene and InGaAs are placed on an HR-Si/SiO₂ substrate so that is possible to gate-tune the graphene conductivity and measure the THz emission variations due to the graphene tuning.

Since the PCAs cannot be integrated inside chips, for a proper demonstration of the THz emission of graphene antennas for the purpose of the WiPLASH project, all-electronic antennas were developed, simulated, and characterized. Additionally, a novel antenna patch design was conceptualized where the radiating element consists of a stack of graphene/dielectric/graphene. Like this, the patch antenna can be gate-tunable when a bias between the two graphene patches is applied.

For the completion of the last activity of WP1 and the present report, graphene patch antenna arrays were designed and simulated. The low THz emission of the graphene antenna can then be compensated by the antenna array presented in this report. Beam-steering can be accomplished by phase delay of the excitation signals for each antenna.

2 Graphene-based Antenna Measurements

Several graphene antennas were manufactured by AMO (WP2) and characterized by UoS in order to prove THz emission and tuning. Initial measurement results were already reported in deliverable D2.1 First Co-integration of Graphene Antennas with Full Custom SiGe Transceivers. Details about the latest antenna characteristics and measurement results are described in this chapter. An acrylic box was built around the THz-TDS setup for measurements of the samples in an N_2 environment (Figure 1).

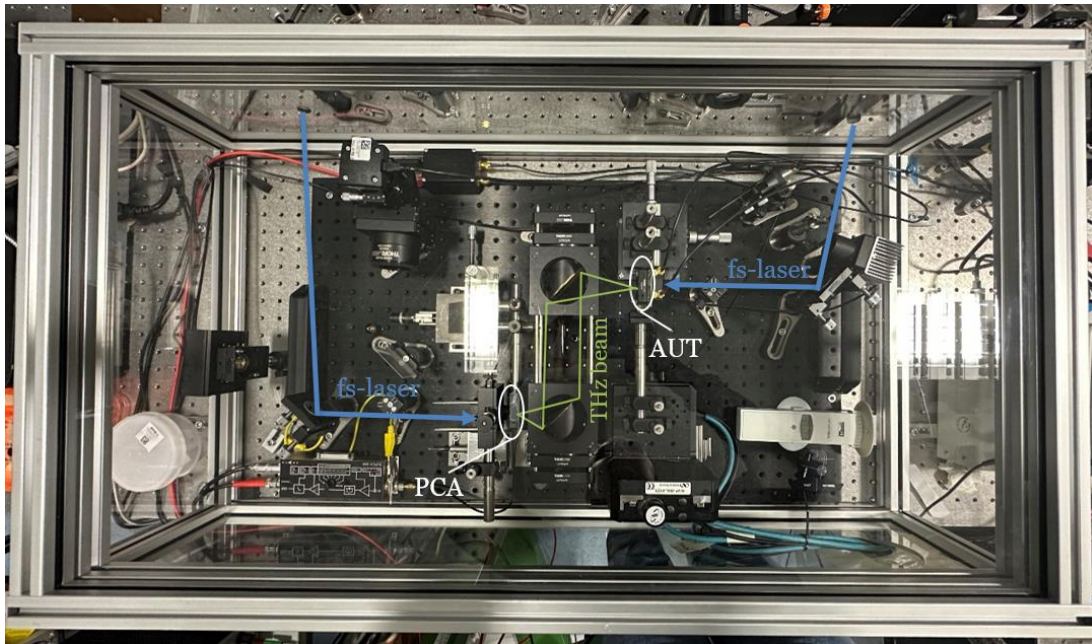


Figure 1: THz-TDS measurement setup inside a box for N_2 environment measurements

2.1 Optically Excited Graphene-based Dipole Antenna

Throughout the project duration, several dipole PCAs were developed and characterized. An overview of the samples can be seen in Figure 2 which shows a metallic dipole PCA (Figure 2a) - always used for comparison purposes, a standard graphene dipole (Figure 2b), a graphene dipole with graphene conduction lines, and a graphene dipole with a metal piece in the vicinity of the dipole gap. The different designs were developed so that it was possible to decrease as much as possible the THz emission of the conduction lines (Figure 2c) and to force the charge carriers generated in the dipole gap to travel to the graphene dipole (Figure 2d).

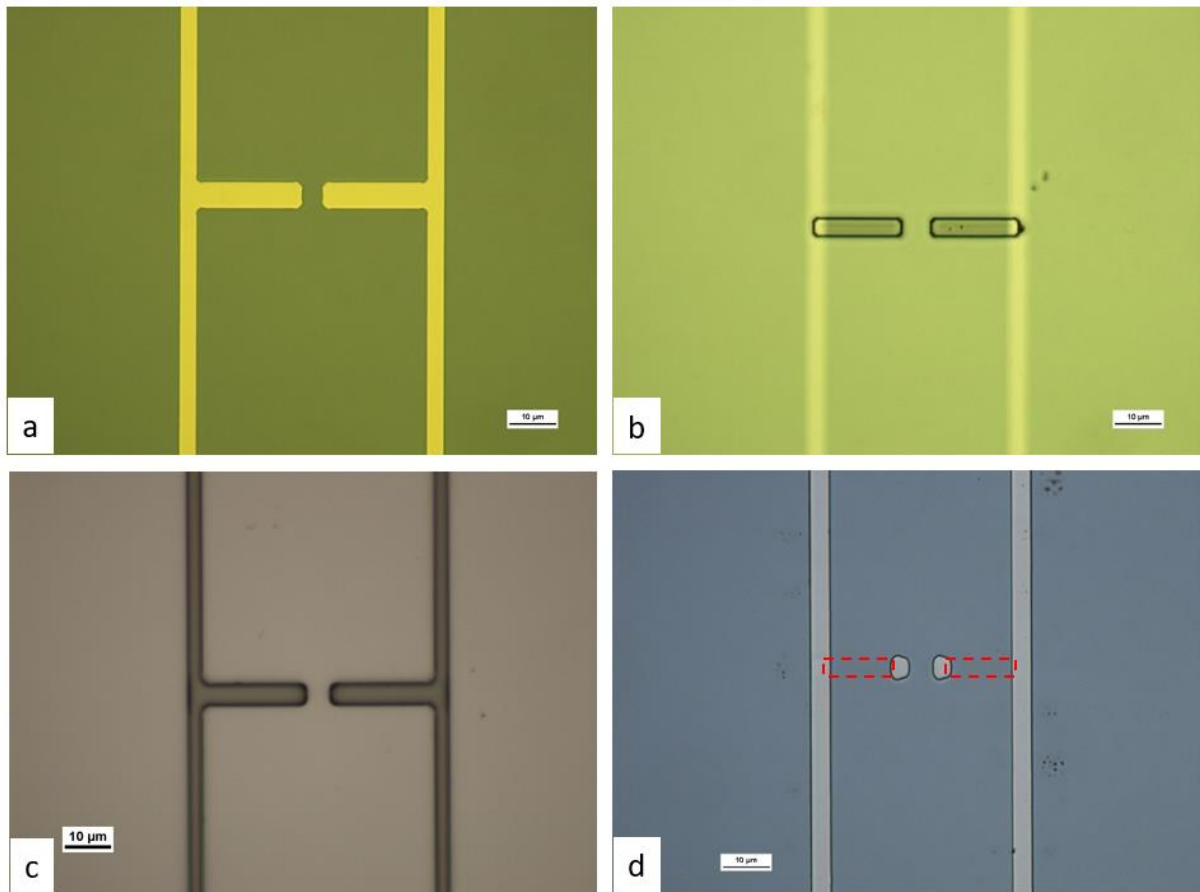


Figure 2: Different dipole PCA designs with (a) metal dipole, (b) standard graphene dipole, (c) graphene dipole with graphene conduction lines, and (d) graphene dipole with metal close to dipole gap

THz emission from the antenna of Figure 2d was measured and to confirm that the emission was due to the graphene dipole arms and not from conduction lines, the optical excitation with the fs-laser was focused in the regions below and above the dipole gap. It is clear a THz emission from the area where the graphene dipole is (Figure 3).

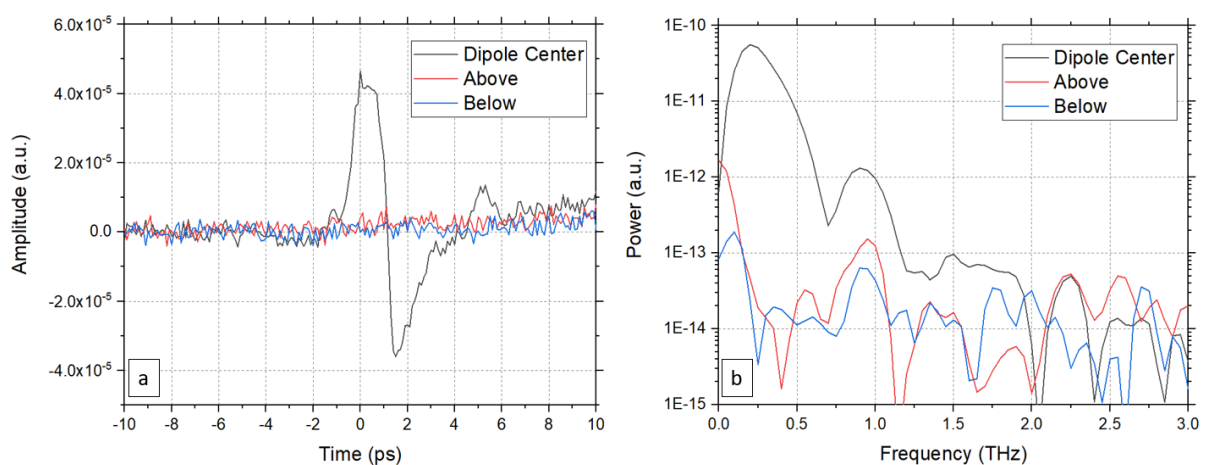


Figure 3: THz emission measurements of the graphene dipole of Figure 2d with laser excitation spot being in the dipole gap, below and above it with (a) time-domain spectra and (b) frequency-domain spectra

Unfortunately, due to the bias voltage and optical power used (30 V and 10 mW), the graphene antenna was destroyed after a short measurement time. The Figure 4 shows the peak-to-peak value of the THz emission measured in the time-domain over a number of repetitive measurements. The antenna is destroyed after the 20th measurement and it is not possible to measure THz emission from the dipole gap anymore, as can be seen in Figure 5.

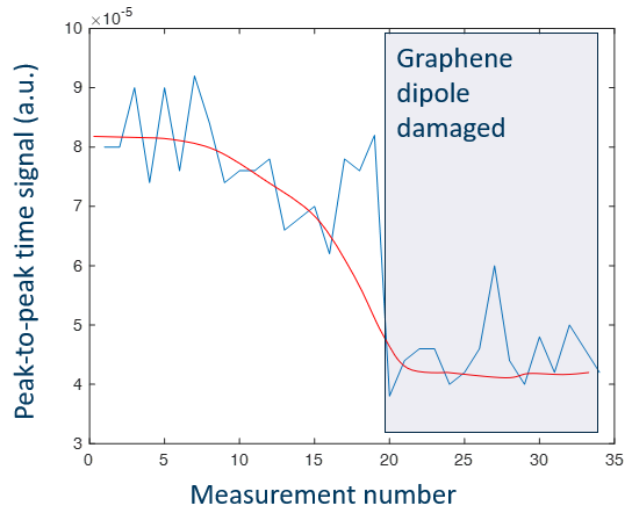


Figure 4: Time-domain peak-to-peak value of the THz emission over repetitive measurements

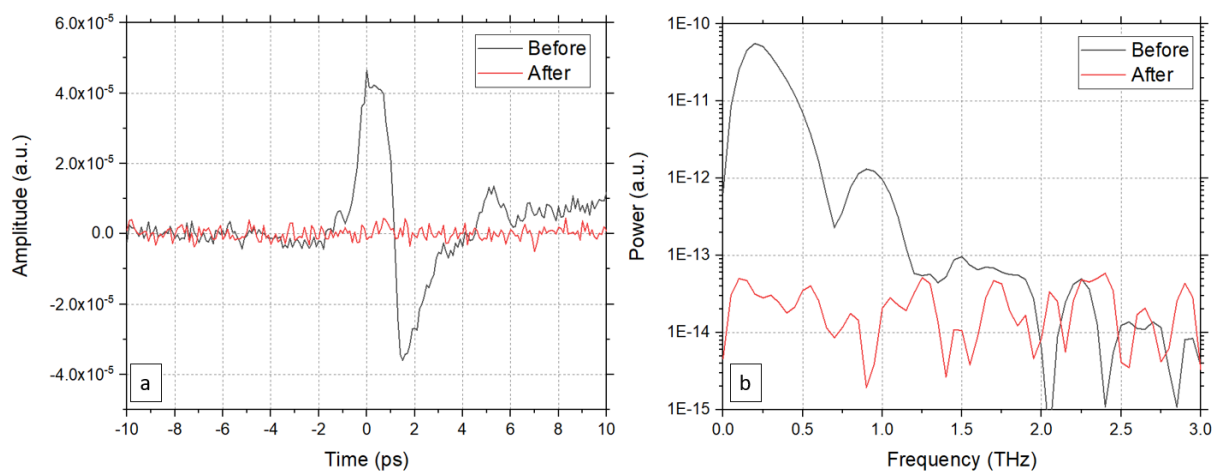


Figure 5: Comparison of the THz emission of the graphene dipole before and after 20 measurements with (a) time-domain spectra and (b) frequency-domain spectra

The damage of the graphene dipole could also be confirmed based on scattering scanning near-field optical microscopy (s-SNOM) imaging taken from before and after THz-TDS measurements (Figure 6).

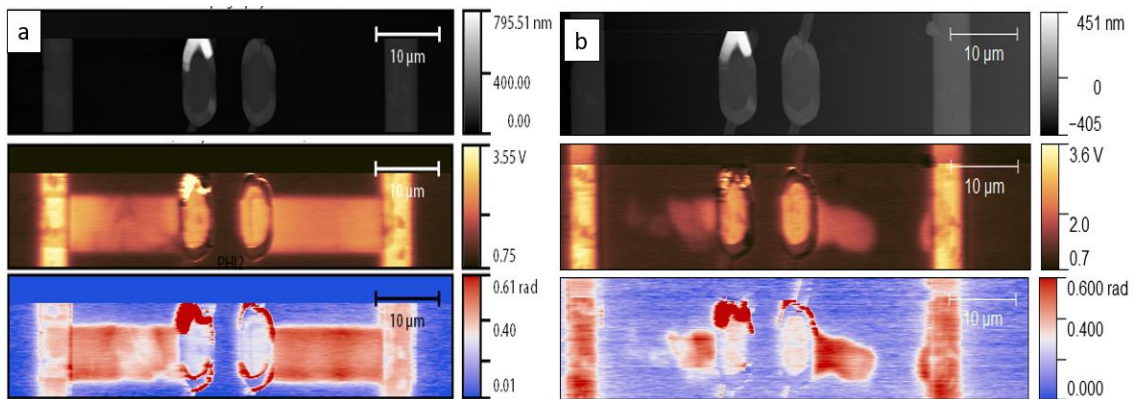


Figure 6: s-SNOM image of the graphene dipole (a) before and (b) after THz-TDS measurements. Top: Topography, centre: E-field amplitude, and bottom: E-field phase

From the s-SNOM image, it is already possible to visualize a difference between the graphene of both dipole arms. As a reminder, a good THz emission of graphene antennas is directly related to the graphene quality. Lower optical power and bias voltage lead to a lower emission that can prevent the graphene from being destroyed, but at the same time, it reaches the noise level of the measurement setup.

Nevertheless, it is experimentally demonstrated that a graphene dipole PCA on an HR-Si substrate can emit THz radiation.

2.2 Optically Excited Graphene-based Patch Antenna

To demonstrate the tunability of the THz emission with a graphene antenna, a CVD graphene was deposited and patterned to a patch of dimensions of $250\mu\text{m} \times 300\mu\text{m}$ on an HR-Si with 300 nm SiO_2 (Figure 7). An InGaAs emitter with dimensions of $80\mu\text{m} \times 200\mu\text{m}$ was placed on top of the graphene patch. The Measurement setup used was the same as for the antennas of Section 2.1.

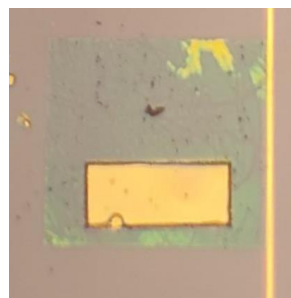


Figure 7: InGaAs emitter on top of the graphene patch antenna. The metal line in contact with the graphene patch is used for biasing graphene by gate-tuning

By focusing the laser beam on the InGaAs, THz radiation is generated and its spectra can be measured. In Figure 8, it is shown the THz measured spectra of InGaAs-only and InGaAs with the graphene patch. It is possible to observe that, even though the overall emission is lower- due probably to a small THz absorption by the graphene, there is a second peak in the time-domain spectra with the graphene patch. The THz emission with InGaAs as an emitter and a graphene patch as an antenna is a totally new experiment and further investigations need to be realized. We believe that the emission, in this case, is a combination of various interactions between the emitted

THz field by the InGaAs and the graphene plasmons. The second peak in the time-domain spectra confirms that graphene is not only acting as a THz absorber, but is also contributing to the THz emitted field.

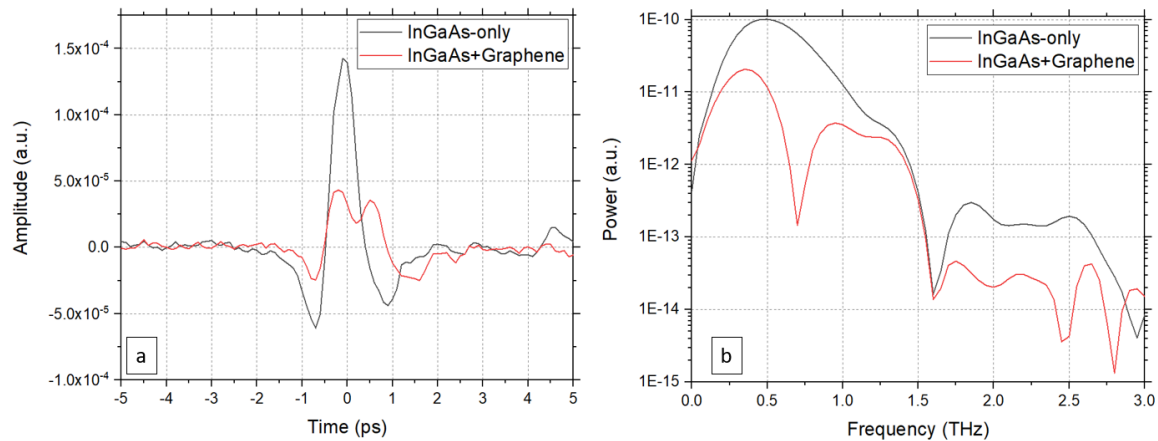


Figure 8: THz emission comparison of only InGaAs and InGaAs on top of graphene with (a) time-domain spectra and (b) frequency-domain spectra

A top contact to the graphene patch and a bottom contact to the HR-Si substrate were made so that it was possible to apply a bias to the graphene and try to gate-tune its conductivity and, consequently, its THz emission spectra. The result is shown in Figure 9, where it is possible to see a clear change in the emission spectra, where the first peak in time-domain decreases while the second peak increases. In the frequency-domain spectra is possible to observe a shift to higher frequencies with the increase in bias.

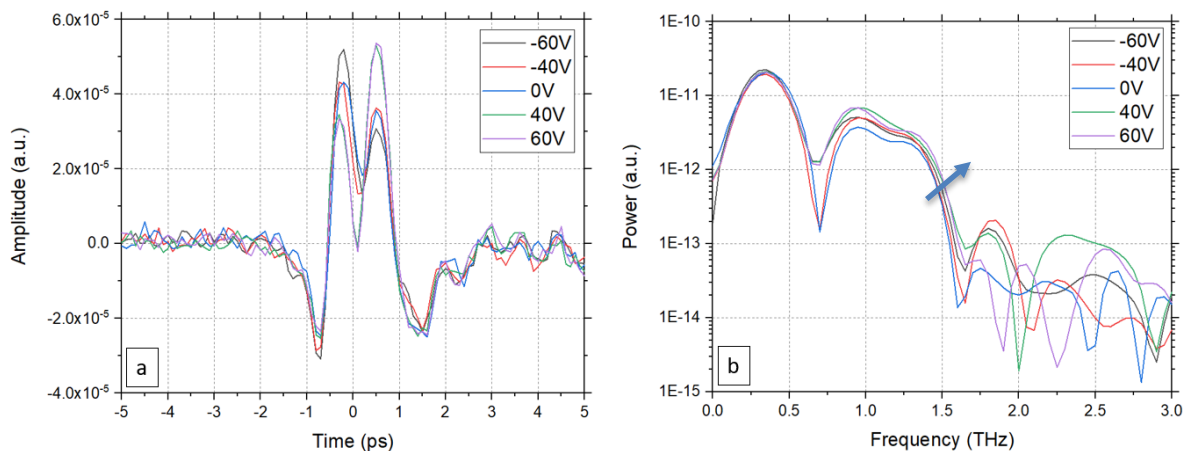


Figure 9: THz emission comparison of InGaAs on top of graphene with different applied bias with (a) time-domain spectra and (b) frequency-domain spectra

With this experiment, we demonstrate the THz tunability of graphene antennas. The THz emission tunability of graphene antennas is highly affected by the graphene quality and the damping of the plasmons along the graphene patch will lead to a low THz emission. To demonstrate better tunability, exfoliated graphene patches, which are expected to have better quality compared to CVD graphene, were also tested in the same manner. By mechanically exfoliating a graphite flake, it was possible to obtain a large bi-layer graphene of dimensions of $\sim 200 \mu\text{m} \times 200 \mu\text{m}$ (Figure 10) and repeat the same measurement procedure.



Figure 10: InGaAs emitter on top of the exfoliated graphene

A metal contact was later done in order to gate-tune the graphene conductivity of the exfoliated flake. The figure Figure 11 shows the THz emission tuning of the exfoliated graphene with InGaAs. A wide change can be observed in the THz emission with applied bias in the time-domain spectra and a big shift in the frequency-domain.

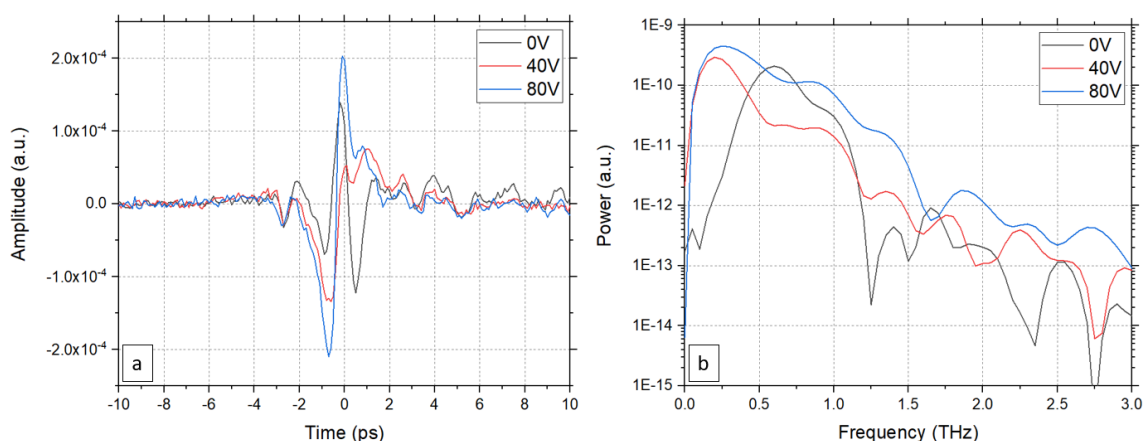


Figure 11: THz emission comparison of InGaAs on top of exfoliated graphene with different applied bias with (a) time-domain spectra and (b) frequency-domain spectra

With this, we show tuning of the THz emission by electrostatic tuning the graphene conductivity by a gate voltage and that high-quality graphene is needed for the sake of THz experiments. Unfortunately, high-quality exfoliated graphene flakes are not yet manufactured on a large scale and will not provide big graphene areas, which limits the experiments.

2.3 All-electronic Excited Graphene-based Patch Antenna

For the purpose of WiPLASH project, it was designed an all-electronic antenna to operate between 220 – 325 GHz that could be easily integrated. More details about the antenna dimensions and simulation results can be found in deliverable D1.2 Graphene Integration Design Report. Additionally, to show THz emission tuning, a second design, which consists of a graphene stack, was developed.

The measurement setup used to characterize these antennas is a combination of VNA with frequency extenders reaching the frequency band of 220 - 325GHz. A GSG probe tip provides the signal from the frequency extender to the AUT, and a standard horn antenna placed perpendicular to the AUT at a distance of 25 cm is used to detect the emitted radiation from it at the radiation angle of 0° (Figure 12). With this setup is possible to measure the S11 and S21 and calculate the gain of the AUT.

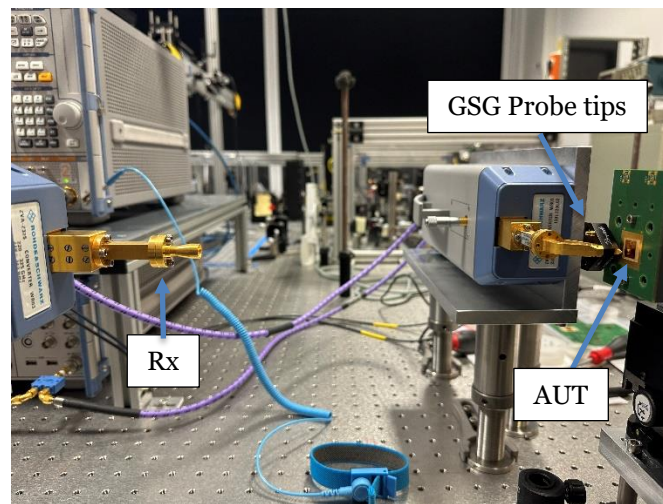


Figure 12: VNA setup for characterization of all-electronic patch antennas

2.3.1 Graphene Monolayer Patch Antenna

The patch antennas manufactured by AMO are shown in Figure 13. In the first trials, a metal patch antenna with the same dimensions as the graphene patch antenna was measured for comparison reasons. The patch antennas were fabricated on a polyimide substrate of 50 μm thickness and GSG contact pads made of palladium were deposited for the contact with the RF probe tip. A metallization on the back side of the substrate was done using aluminum.

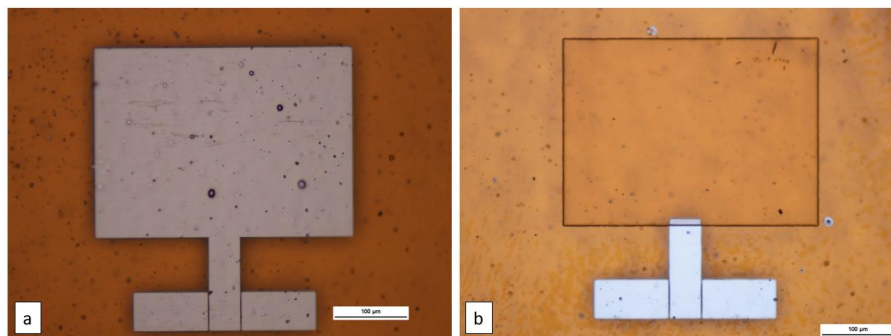


Figure 13: Patch antennas in polyimide substrate with (a) standard metal patch antenna and (b) graphene patch antenna

Measurement results show that the metal antenna resonates at the band as expected at around 295 GHz with a gain of 3.6 dB. The shift of the resonance to a higher value than expected, which was 280 GHz, can be explained by the real dielectric constant of the substrate that is higher than used for the simulations and the probe tip contact with the GSG pads that can also alter the matching.

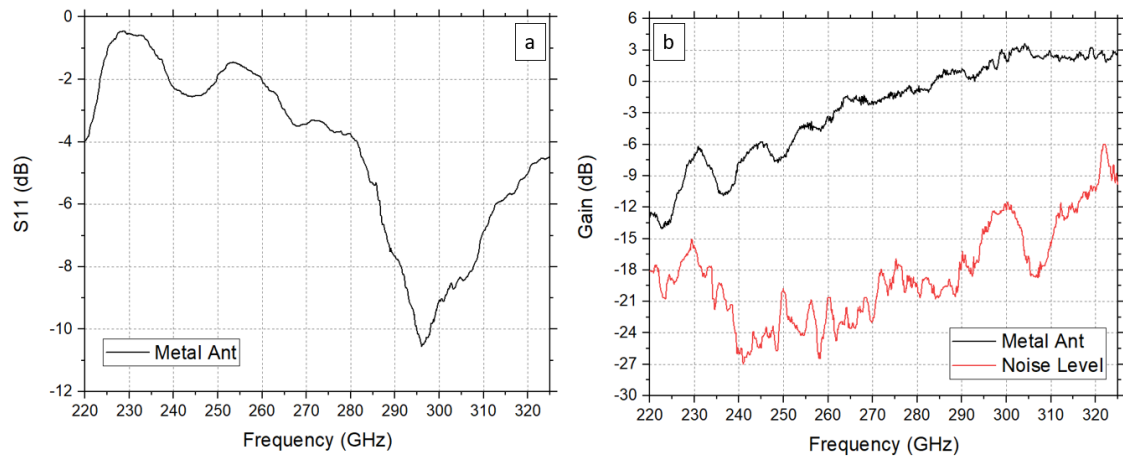


Figure 14: Measured values of (a) S_{11} and (b) gain of the metal patch antenna

By theory and previous simulations, the graphene patch antennas should present a lower resonance frequency compared with the metal antenna with the same dimensions. Previous reported simulation results shown in Deliverable D1.2 states that for a graphene antenna, the resonance frequency is smaller than for the metallic patch antenna and it depends on the chemical potential of graphene and relaxation time. It is difficult to stipulate preliminarily what is the resonance frequency of such antennas because the chemical potential of graphene used and also the relaxation time when transferred to polyimide is not precisely known. From our measurements, it is not possible to see deep in the S_{11} values for the graphene patch antennas. As a reminder already stated in the previous report, good antenna behavior (less than -10 dB for S_{11}) will only be achieved with a very high graphene quality material.

The far-field gain calculated from the S_{21} values shows just a slight difference when compared to the GSG signal emission. Still from Figure 15, it is possible to observe that the sample with a graphene patch receives more of the signal compared with the sample without a patch for the higher frequency range. Also, it is possible to observe a small increase in the gain when using the graphene patch for these frequencies (from 288 GHz).

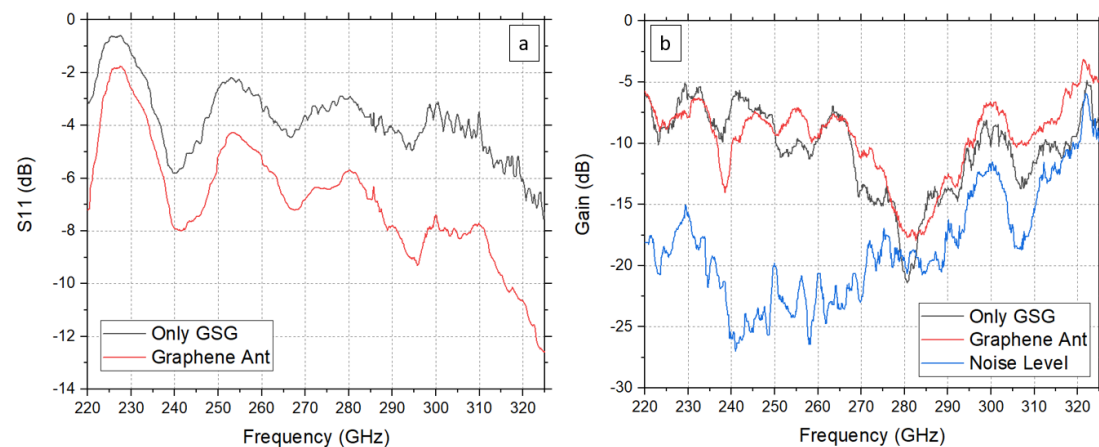


Figure 15: Measured values of (a) S_{11} and (b) gain of the graphene patch antenna

Even though the emission is very small, this is the first demonstration of THz emission from a single-layer CVD graphene antenna at this frequency range.

2.3.2 Graphene Monolayer hBN Embedded Patch Antenna

The graphene material is extremely affected in its electrical properties by its surroundings and by the substrate. For that reason, some graphene antennas were manufactured where the graphene is embedded in between two CVD hBN layers to shield the graphene from the effects of the environment (Figure 16).

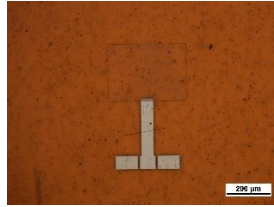


Figure 16: CVD hBN/CVD graphene/CVD hBN patch antenna

The measurement results of the graphene embedded in hBN patch antennas are as follows (Figure 17).

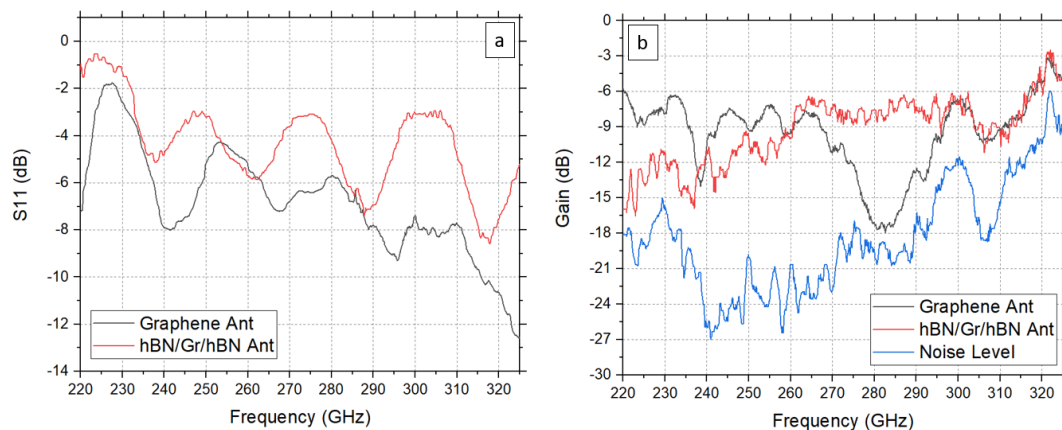


Figure 17: Measured values of (a) S_{11} and (b) gain of the graphene embedded in hBN patch antenna

The measurements show that, even though the S_{11} is compromised, there is an improvement in far-field emission with a clear emission from the antenna in the range of 265 – 300 GHz, demonstrating THz emission from graphene antennas and that this emission can be improved by shielding the graphene with hBN.

2.3.3 Graphene Stack Patch Antenna

For demonstration of THz tuning from the all-electronic patch antennas, a new antenna design was conceptualized, where it is possible to gate-tune the graphene conductivity by using a second graphene patch on top of it, which is separated by a dielectric (Figure 18). The dielectric on top of the bottom graphene patch is used for the purpose of top gate tuning and the top graphene patch is used as a THz-transparent bias contact, as well as to increase the overall emission of the antenna. A bias voltage can be applied between the two graphene patches will cause the tuning of the THz

emission from the antenna.

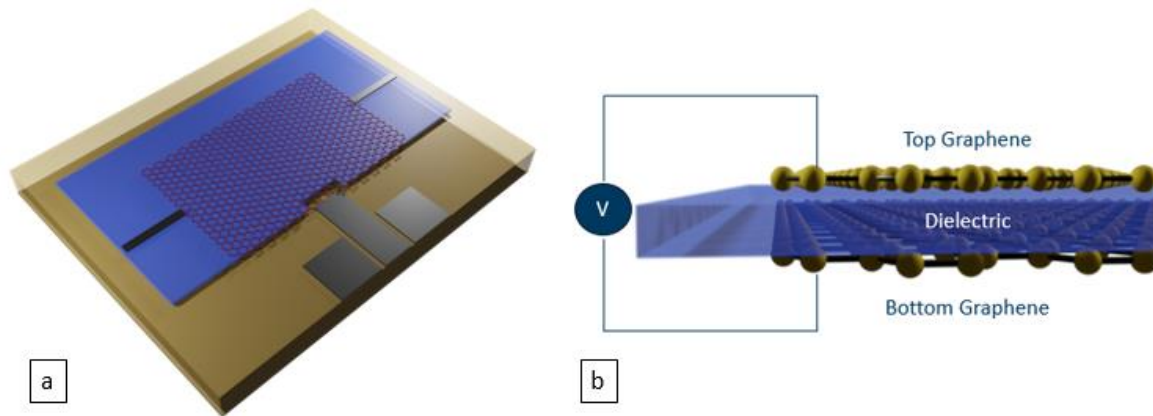


Figure 18: Graphene stack patch where (a) is the proposed design and (b) is a demonstration of the graphene tuning.

Not only the emission is increased but it is also possible to tune the resonance frequency by a bias applied to the antennas, as can be seen in Figure 19.

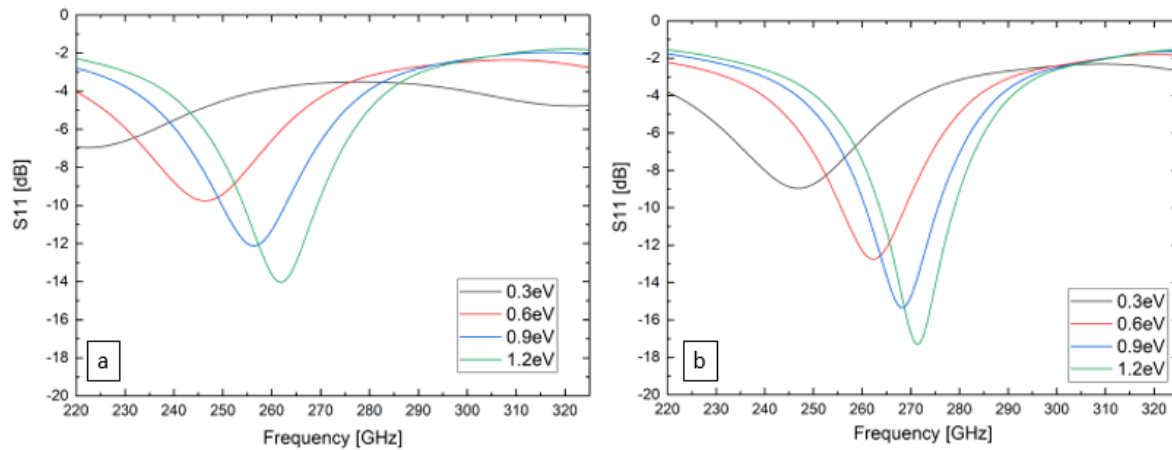


Figure 19: S_{11} parameter of the patch antenna with graphene of different chemical potentials (that can be modified with the bias) and 1.2ps of relaxation time for (a) a standard monolayer antenna and (b) for the proposed antenna stack.

Even with a resonance frequency change compared to a standard monolayer graphene patch antenna, a graphene/dielectric/graphene stack as a radiating element enables the supplying of a bias to the graphene to modify its conductivity. Also, the 2-layer graphene stack, as already studied by others, provides a conductivity that is two times higher than for single-layer graphene. This will lead to alleviation in the mobility values required for a graphene patch to act as an antenna, as can be seen in Figure 20.

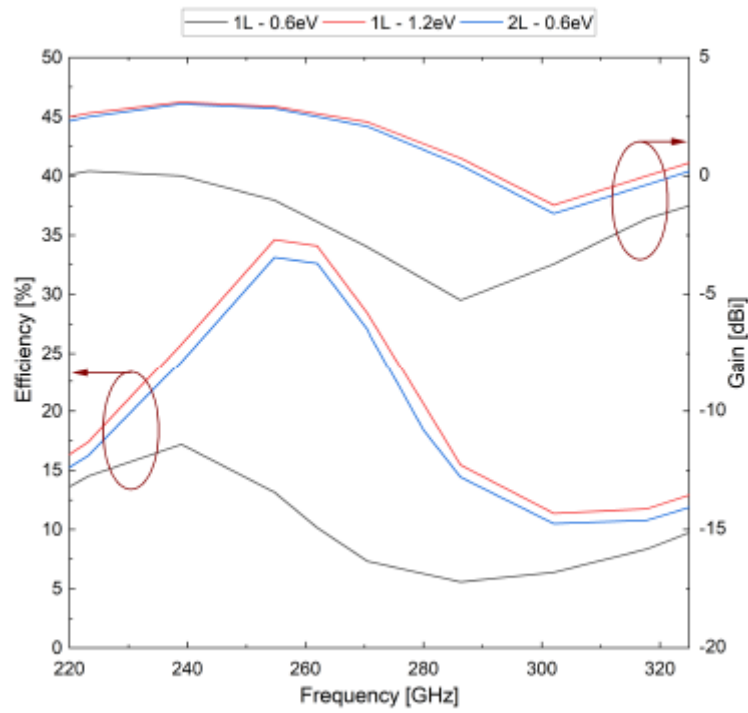


Figure 20: Efficiency and gain comparison of a standard single-layer graphene antenna and the proposed graphene stack

The efficiency and gain for the stack graphene antenna are the same for a single-layer graphene antenna with double its chemical potential.

3 Graphene-Based Antenna Arrays Simulations

To increase the THz emission of the graphene antennas, antenna arrays can be implemented. Here we report simulation results of graphene antenna arrays for the dimensions of the measured antennas of the last chapter.

Different antenna array configurations were simulated with different numbers of antenna elements and spacing between them.

For the initial study of the number of antenna elements in the array, a spacing of $\lambda/2$ was kept between each edge of the antenna patch.

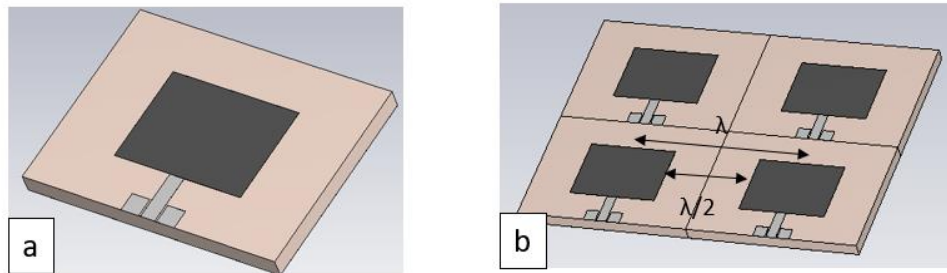


Figure 21: Example of the antenna array simulation in CST with (a) single antenna and (b) 2x2 antenna array

Due to the low values of far-field gain of graphene patch antenna due to low graphene quality, high-quality graphene (1.2 ps relaxation time and 1.2 eV of chemical potential) was used for simulations for a better comparison in the improvement of radiation using arrays.

Following the simulation, the result of the far-field gain is shown in Figure 22. For a single antenna, the far-field gain is 2.7 dBi at the resonance frequency. When using 2 x 2, 3 x 3, and 4 x 4 antenna arrays, this value increases to 6.5 dBi, 10.9 dBi and 13.2 dBi, respectively. For all cases, the main lobe direction was kept at 0° .

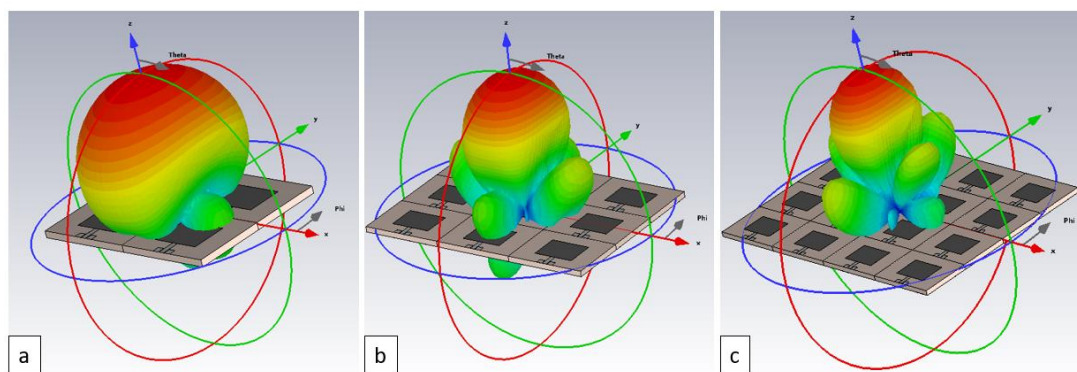


Figure 22: simulated 3D pattern of the far-field gain of the antenna arrays

For beam steering evaluation capabilities, the 2 x 2 antenna array was used and a phase delay in the input signal to the antennas was applied.

The beam steering due to phase delay between the input signals for each antenna was simulated for the case of a delay of 20° between each antenna and also for a phase delay of 45° between the input signals. The main lobe direction changes from 0° to -

13° and -25° for the two cases mentioned but keeping the 6.5 dBi of gain as for the case of 0° phase delay. (Figure 23).

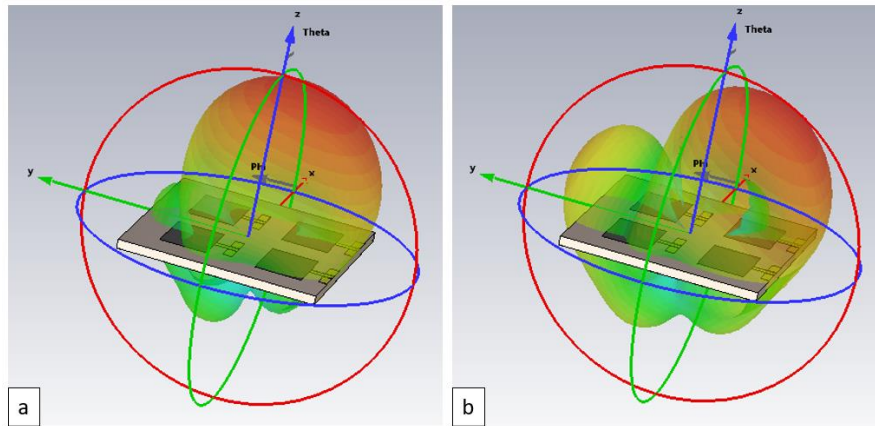


Figure 23: Simulated 3D far-field pattern for the antenna array when (a) an input phase delay of 20° between antennas and (b) an input phase delay of 45° between antennas

It was also studied if graphene with low relaxation time would limit the beam steering capabilities of the antenna array. The same array was simulated with a relaxation time of 0.3 ps, but simulation results show that the beam steering capability is kept but with a low far-field gain of 0.9 dBi for no beam-steering - as already expected for graphene with lower quality, and of 0.6 dBi when there is a phase delay in the input signal (Figure 24).

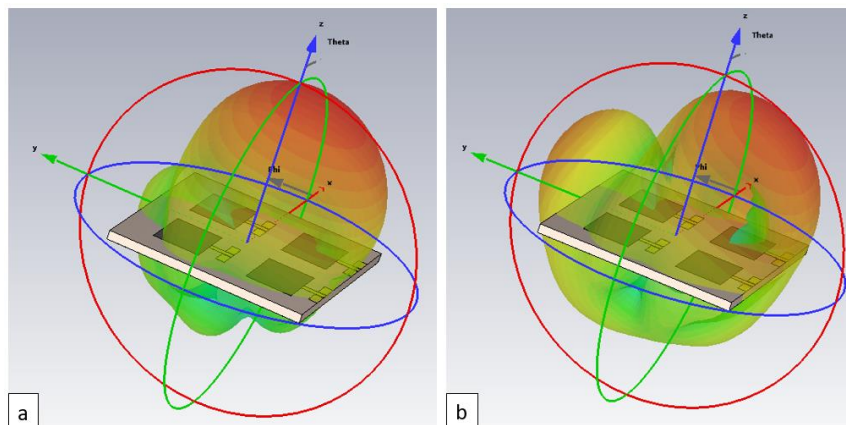


Figure 24: Simulated 3D far-field pattern for the antenna array with 0.3ps of relaxation time when (a) an input phase delay of 20° between antennas and (b) an input phase delay of 45° between antennas

By further increasing the delay between the input signals, for this specific array configuration, a second radiation beam starts to appear in the opposite direction of the main beam. A second radiation beam can be used for multipath communications.

In this chapter, we have shown the possible capabilities of graphene antenna beam steering by phase delay input. Still here, the overall antenna array far-field gain is dependent on the graphene quality.

4 Summary of Results

This deliverable was focused on demonstrating the capabilities of graphene antennas to resonate at THz frequencies and to show the THz tunability of such antennas. Thus, the University of Siegen (UoS) designed, simulated, and characterized several graphene antennas. Through various experiments, based on different excitations (optical and electrical) and measurement techniques (THz-TDS and VNA), a variety of graphene antennas was proven to emit tunable THz radiation, which was measured at far-field.

We first focused on proving THz emission of photoconductive dipole antennas. Based on the principles of a standard THz-TDS system, the traditional antenna emitter was replaced by a graphene dipole antenna. Due to the very low THz emission of the graphene antenna, new concepts had to be developed, leading to a final design of a graphene dipole photoconductive antenna with a metal inset close to the dipole gap. This new design was able to overcome the very low charge carrier mobility in the graphene material used for the antennas and THz emission was measured. In this configuration, tuning of graphene conductivity was not possible.

Subsequently, in order to demonstrate THz emission tunability, a new concept with a bias-free THz photoconductive antenna was developed. The bias-free THz emitter was an InGaAs placed on top of a graphene patch to act as a THz antenna. An effect of graphene on the overall THz emission was measured and by using a gate voltage, it was possible to demonstrate the change in THz emission based on graphene conductivity tuning. The cut-off frequency of the graphene antenna was shifted to higher values with higher applied voltages. The small tuning capability in this experiment can be explained by the low mobility of the CVD graphene used as an antenna. An exfoliated graphene antenna was used for the same experiments and the tuning of THz emission was clearly higher.

Thereafter, to demonstrate the THz emission and THz tunability of an integrable antenna, an all-electronic-based graphene patch antenna was designed. The antenna was designed to resonate in the range of 220 - 325GHz. Due to the very large dimensions of the antenna for this frequency range, only CVD graphene was used. The graphene patch antenna showed a very small THz emission in this frequency range. As a reminder, at the given achievable CVD graphene material characteristics, antenna behavior presents many limitations. In order to improve the CVD graphene materials characteristics, a CVD graphene patch embedded in CVD hBN was characterized and it was possible to measure an even higher emission from the antenna in this frequency region.

Finally, a last antenna concept was developed to demonstrate the THz emission tuning of an all-electronic graphene patch antenna. This antenna consists of a stack of graphene/dielectric/graphene, where a bias voltage is applied between the two graphene patches, and, with this, the THz emission of the antenna can be tuned. The proposed graphene stack antenna enables not only resonance frequency tuning but also provides a means of changing the conductivity of graphene at the same time alleviating, to some extent, the requirements of high mobilities.

For the completion of this report, graphene patch antenna arrays were studied by simulations. The low emission of the graphene patch antenna can be compensated by using antenna arrays. Additionally, antenna arrays give rise to the beam steering possibility, as also described in this report, leading to extra usages for the graphene antenna, such as multi-channel communications. The size reduction of graphene antennas compared to metal antennas can, here, be compromised by the use of

arrays. Nevertheless, the advantage of graphene antennas at THz frequencies is still present in the possibility of resonance frequency tuning without changing the dimensions of the antennas, as it is not the case for standard metal antennas.

Bibliography

- [1] S. Abadal, R. Guirado, H. Taghvaei, A. Jain, E. Pereira de Santana, P. Haring Bolívar, M. Saeed, R. Negra, Z. Wang, K.-T. Wang, M. C. Lemme, J. Klein, M. Zapater, A. Levisse, D. Atienza, D. Rossi, F. Conti, M. Dazzi, G. Karunaratne, I. Boybat and S. Abu, "Graphene-based Wireless Agile Interconnects for Massive Heterogeneous Multi-chip Processors," *IEEE Wireless Communications*, 2022.
- [2] J. Klein, A. Levisse, G. Ansaloni, D. Atienza, M. Zapater, M. Dazzi, G. Karunaratne, I. Boybat, A. Sebastian, D. Rossi, F. Conti, E. P. de Santana, P. Haring Bolívar, M. Saeed, R. Negra, Z. Wang, K.-T. Wang, M. C. Lemme, J. Akshay, R. Guirado, H. Taghvaei and S. Abadal, "Architecting more than Moore: wireless plasticity for massive heterogeneous computer architectures (WiPLASH)," in *CF '21: Proceedings of the 18th ACM International Conference on Computing Frontiers*, 2021.
- [3] E. Pereira de Santana, A. K. Wigger, Z. Wang, K.-T. Wang, M. Lemme, P. Haring Bolívar and S. Abadal, "Integrated Graphene Patch Antenna for Communications at THz Frequencies," in *2022 47th International Conference on Infrared, Millimeter and Terahertz Waves (IRMMW-THz)*, 2022.
- [4] I. Llatser, C. Kremers, A. Cabellos-Aparicio, E. Alarcón and D. N. Chigrin, "Comparison of the Resonant Frequency in Graphene and Metallic Nano-antennas," in *AIP The Fifth International Workshop on Theoretical and Computational Nano-Photonics*, 2012.
- [5] W. Yu, Y. Zhao, L. Brus, K. Kim and P. Kim, "Tuning the Graphene Work Function by Electric Field Effect," *Nano Letters*, vol. 12, 2010.
- [6] I. Llatser, C. Kremers, A. Cabellos-Aparicio, J. M. Jornet, E. Alarcón and D. N. Chigrin, "Graphene-based nano-patch antenna for terahertz radiation," *Photonics and Nanostructures - Fundamentals and Applications*, vol. 10, no. 4, pp. 353-358, 2012.
- [7] I. Llatser, C. Kremers, D. N. Chigrin, J. Miquel Jornet, M. C. Lemme, A. Cabellos-Aparicio and E. Alarcón, "Radiation characteristics of tunable graphennas in the terahertz band," *Radioengineering*, 2012.
- [8] T. Tamagnone, J. S. Gómez-Díaz, J. R. Mosig and J. Perruisseau-Carrier, "Reconfigurable terahertz plasmonic antenna concept using a graphene stack," *Appl. Phys. Lett.*, 2012.
- [9] S. Dwivedi and S. Chandra, "Design and Simulation of Graphene Based Antenna for Radiation Pattern," in *2021 6th International Conference for Convergence in Technology (I2CT)*, 2021.
- [10] N. M. Burford and M. O. El-Shenawee, "Review of terahertz photoconductive antenna technology," *SPIE Opt. Eng.*, vol. 56, 2017.
- [11] V. Apostolopoulou and M. E. Barnes, "THz emitters based on the photo-Dember effect," *Physics D: Applied Physics*, vol. 47, 2014.